iScience

CellPress
OPEN ACCESS

Article

Ultrafast observation of the abnormal time delay of femtosecond laser pulses in a quartz crystal

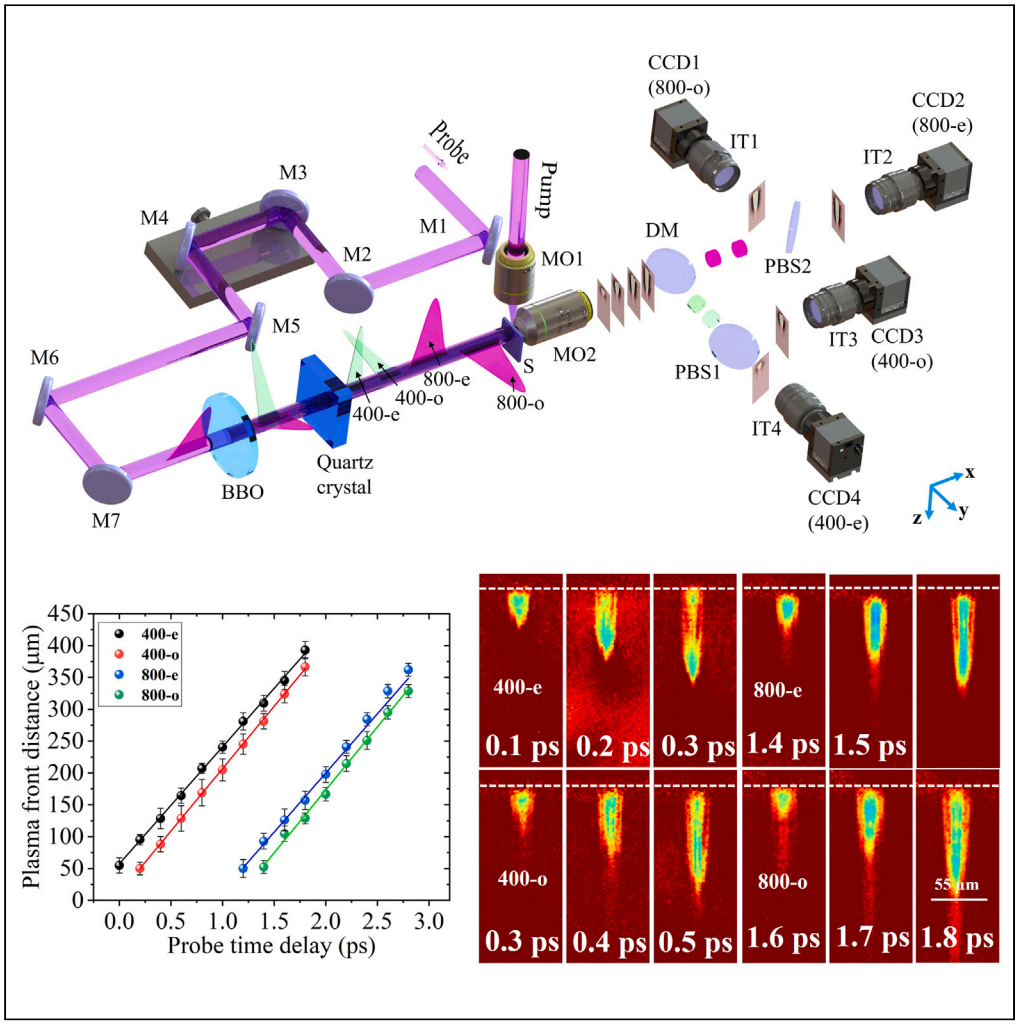

Baoshan Guo,
Tianyong Zhang,
Lan Jiang

gbs@bit.edu.cn (B.G.)
jianglan@bit.edu.cn (L.J.)

Highlights

Designed and built an ultra-fast multi-frame observation system

Discovered an energy-independent abnormal time delay of fs laser pulses

Observed and measured the time intervals between subpulses

Continuously observed the temporal evolution of multiple plasma shock waves

Guo et al., iScience 27, 110316
July 19, 2024
https://doi.org/10.1016/j.isci.2024.110316

iScience

CellPress
OPEN ACCESS

Article

Ultrafast observation of the abnormal time delay of femtosecond laser pulses in a quartz crystal

Baoshan Guo,[1,2,5,*] Tianyong Zhang,[1,4] and Lan Jiang[1,2,3,*]

SUMMARY

Light with different frequencies has different propagation speeds when propagating in a medium. Nonlinear optics indicates that the refractive index of the medium also varies with the intensity of light. In this article, we have discovered an anomalous slow light phenomenon that is independent of light intensity through multi-frame ultrafast imaging. The experimental results show that when coaxial 800-nm and 400-nm pulses simultaneously enter the quartz crystal, the time delay between the 800-nm and 400-nm laser pulses is up to 5 times the normal value calculated by the dispersion theory. Moreover, this delay is independent of the laser intensity, indicating that the anomalous slow light phenomenon does not originate from refractive index changes in nonlinear optics. This abnormal time delay effect may find more applications in different fields, and its physical mechanism still needs further exploration.

INTRODUCTION

In linear optics, the rate of weak light passing through a medium is independent of light intensity.[1,2] The refractive index $n(\omega)$ is different for light of different frequencies, which is known as the dispersion effect.[3] Under normal dispersion, the refractive index of high-frequency (short-wavelength) light is high and the propagation speed is low.[4] For strong light, if the electric field strength of the light wave is greater than the Coulomb field inside the atom, nonlinear phenomena will occur.[5] The change in refractive index of the material caused by electronic polarization in the material, called nonlinear optical phenomenon, is related to the high-order power E^n of the laser electric field, and the change in refractive index further affects the speed of light propagation.[6,7] For example, the optical Kerr effect ($\Delta n \propto E^2$) in a strong laser field, the change in refractive index of a material Δn is proportional to the square of the laser electric field E^2, which is also the laser intensity I .[8–11] At present, a large number of experimental studies on light deceleration or light regulation rely on the regulation of the refractive index of materials by the intensity of pump light.[12–20]

In this study, we experimentally measured the anomalous time shift of femtosecond laser pulses in quartz crystals. For the 800-nm and 400-nm laser pulses entering the quartz crystal simultaneously and coaxially, the time delay between the two output pulses is up to five times the theoretical calculation value of dispersion. In other words, the excitation of the 800-nm pulse caused the propagation speed of the subsequent 400-nm laser pulse to significantly slow down, resulting in an abnormal time shift between the two pulses. We used single-shot multi-frame imaging technology to measure the time interval between subpulses and verified that this abnormal time shift phenomenon is not caused by general nonlinear effects, as it is independent of pulse intensity. That is to say, the refractive index of quartz crystals has not changed ($\Delta n = 0$). This indicates that the additional time delay of the laser pulse we discovered is not caused by changes in the refractive index of the material. And this time shift is very stable, which can be used to control the pulse delay time precisely. We used a pulse sequence with time offset to continuously detect the evolution process of laser-induced plasma shock waves at frame intervals of 200-fs and 1.1-ps, revealing the coupling effects between multiple plasma shock waves.

Principle and equipment

Generation of subpulses with different polarizations and wavelengths

A light-splitting scheme was applied to generate different laser pulses, and Figure 1 illustrates the principle underlying this scheme. Two nonlinear crystals, β-barium borate (BBO) and quartz crystals, were used in the pulse generation process. A BBO crystal is a negative-uniaxial material with type-I phase matching. A fundamental-frequency laser is an ordinary ray (o-ray) and obeys the principle of refraction, whereas a

[1]Laser Micro/Nano Fabrication Laboratory, School of Mechanical Engineering, Beijing Institute of Technology, Beijing 100081, P.R. China
[2]Yangtze Delta Region Academy of Beijing Institute of Technology, Jiaxing 314000, P.R. China
[3]Beijing Institute of Technology Chongqing Innovation Center, Chongqing 401120, P.R. China
[4]Beijing Academy of Science and Technology, Beijing 100089, P.R. China
[5]Lead contact
*Correspondence: gbs@bit.edu.cn (B.G.), jianglan@bit.edu.cn (L.J.)
https://doi.org/10.1016/j.isci.2024.110316

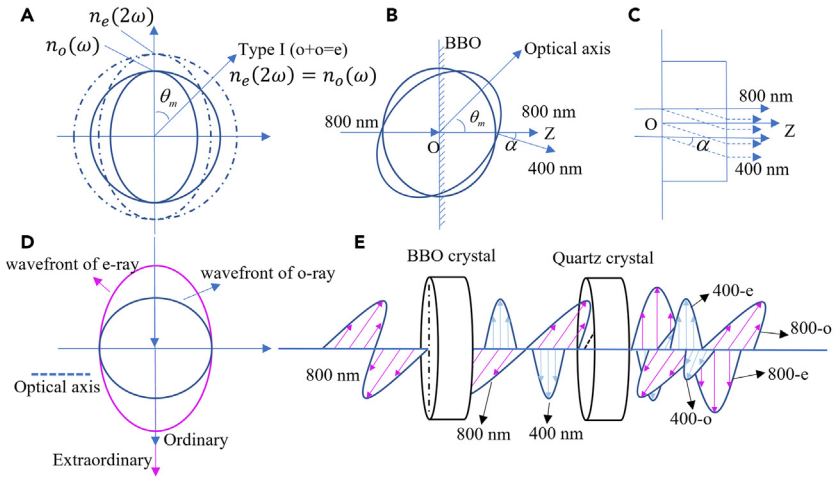

Figure 1. Principle of multipulse generation

(A–C) Phase matching and angle deviation in a BBO crystal.

(D) Birefringence of a quartz crystal.

(E) Generation of four probe subpulses. The circles represent the wavefront of an ordinary ray (o-ray), and the ellipses represent the wavefront of extraordinary ray (e-ray) in (A), (B) and (E).

frequency-doubled laser is an extraordinary ray (e-ray) that does not obey this principle.[21] The o-ray is vertically polarized, whereas the e-ray is parallel polarized. Accordingly, when a femtosecond laser pulse with a single polarization passed through the BBO crystal, it was frequency doubled by the crystal; therefore, the fundamental-frequency and frequency-doubled lasers were noted to be two linearly polarized perpendicular pulses. The refractive index values for 800- and 400-nm laser pulses traveling through the BBO crystal could thus be derived according to the Sellmeier equation[22] as follows:

$$n_o^2(\lambda) = 2.7359 + \frac{0.01878}{\lambda^2 - 0.01822} - 0.01354\lambda^2 \quad \text{(Equation 1)}$$

$$n_e^2(\lambda) = 2.3753 + \frac{0.01224}{\lambda^2 - 0.01667} - 0.01516\lambda^2 \quad \text{(Equation 2)}$$

where λ is the incident wavelength of the laser (μm), n_o is the refractive index of the o-ray, and n_e is the refractive index of the e-ray.

The two outgoing pulses were determined to have a time delay owing to the phase velocity mismatch BBO phase matching. To overcome this, phase matching must be performed by adjusting the BBO optical axis to a specific angle in accordance with the polarization vector of the fundamental-frequency laser. As illustrated in Figure 1A, the refractive index equation is $n_o^{\omega} = n_e^{2\omega}(\theta_m)$, where θ_m is the phase-matching angle. The phase-matching equation is as follows:[23]

$$sin^2\theta_m = \frac{n_e^2(2\omega)\left[n_e^2(2\omega) - n_o^2(\omega)\right]}{n_o^2(\omega)\left[n_o^2(2\omega) - n_e^2(\omega)\right]} \quad \text{(Equation 3)}$$

By combining Equations 1 and 2, we calculated the refractive index values for the 800- and 400-nm pulses to be 1.6606 and 1.5679, respectively. Moreover, the phase-matching angle was 29.179°.

As displayed in Figures 1B and 1C, the propagation directions of the 800- and 400-nm pulses differed because the direction of the 400-nm wave vector was inconsistent with the light energy flow; this is known as the spatial walk-off effect. The walk-off angle α can be derived as follows:[24]

$$tan(\alpha) = \frac{1}{2}n_o^2(\omega)\left[\frac{1}{n_e^2(2\omega)} - \frac{1}{n_o^2(2\omega)}\right]\cdot sin^2\,2\theta_m \quad \text{(Equation 4)}$$

We thus calculated the walk-off angle to be 4.3752°. Moreover, on the basis of the thickness of the BBO crystal (0.3 mm), we determined that the distance between the two beams was 0.02 mm, which was noted to be smaller than the beam diameter (8 mm) and could thus be ignored.

In the quartz crystal, a pulse could be split into two pulses with a specific time delay through the birefringence effect. As illustrated in Figure 1D, when the 800- and 400-nm lasers passed through the quartz crystal, four subpulses were generated: an 800-nm ordinary subpulse (800-o), an 800-nm extraordinary subpulse (800-e), a 400-nm ordinary subpulse (400-o), and a 400-nm extraordinary subpulse (400-e). The corresponding refractive index values could be derived as follows,[25]

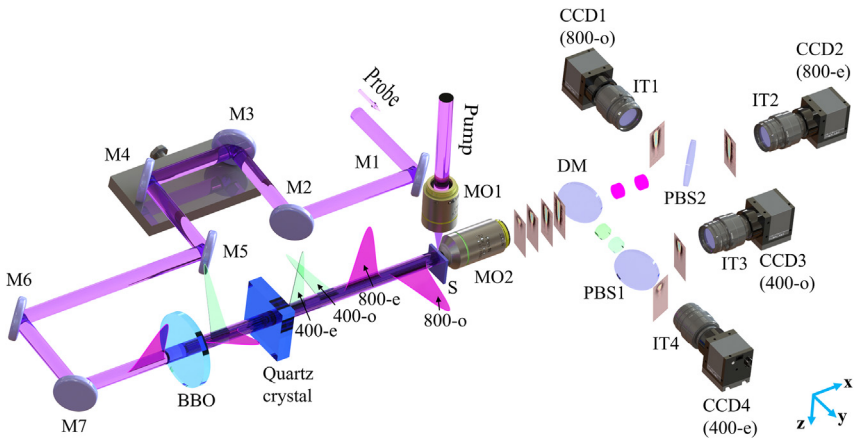

Figure 2. Configuration of the multifrequency pulse framing imaging system

M1–M7: Mirror; BBO: β-barium borate crystal; S: sample; MO1–MO2: microscope objective; DM: dichroic mirror; PBS1–PBS2: polarizing beam splitter; CCD1–CCD4: CCD cameras; IT1-IT4: imaging tube.

$$n_o^2 = 1.28604141 + \frac{1.07044083\cdot\lambda^2}{\lambda^2 - 1.00585997\times10^{-2}} + \frac{1.10202242\cdot\lambda^2}{\lambda^2 - 100} \quad \text{(Equation 5)}$$

$$n_e^2 = 1.28851804 + \frac{1.09509924\cdot\lambda^2}{\lambda^2 - 1.02101864\times10^{-2}} + \frac{1.15662475\cdot\lambda^2}{\lambda^2 - 100} \quad \text{(Equation 6)}$$

The velocity of a laser pulse traveling through an anisotropic material such as a quartz crystal depends on both the phase and group velocities. Owing to the dispersion of laser pulses, group velocity mismatches lead to different traveling times. Hence, the group velocity of subpulses—not the phase velocity—should be used for calculations. In the literature, a conventional formula has been used to calculate the group velocity in birefringent crystals,[26] which is

$$v_g = \frac{c}{n}\left(1 - \frac{\lambda}{n}\cdot\frac{\partial n}{\partial\lambda}\right)^{-1} = \frac{c}{n}\left(1+\frac{\omega}{n}\cdot\frac{\partial n}{\partial\omega}\right)^{-1} \quad \text{(Equation 7)}$$

where c is the velocity of light in vacuum (3.0×10^8 m/s) and n is the refractive index of n_o or n_e.

Therefore, the group refractive index n_g of each subpulse can be used to calculate the propagation time t in the quartz crystal,

$$n_g = c/v_g \quad \text{(Equation 8)}$$

$$t = d\cdot n_g/c \quad \text{(Equation 9)}$$

On the basis of these formulas, we calculated the group refractive index values for the 800-o, 800-e, 400-o, and 400-e subpulses to be 1.5376, 1.5465 1.5572, 1.5668, respectively. By combining the thickness of the crystal (6.4 mm) and the group refractive index, we calculated the propagation times of the 800-o, 800-e, 400-o, and 400-e subpulses to be 3.2802×10^{-11}, 3.2992×10^{-11}, 3.3220×10^{-11}, and 3.3425×10^{-11} s, respectively. The time interval between two adjacent subpulses was noted to be approximately 200 fs (Figure 1E).

Single-shot multiframe imaging system

Figure 2 presents the experimental setup used to separately image the four subpulses. Specifically, a femtosecond Ti:sapphire laser (Spitfire Ace, Spectra-Physics, USA) was used to generate femtosecond pulses. Each of the pulses had a center wavelength of 800 nm, a width of 35 fs, and a repetition rate of 1 kHz. After passing through the beam splitter, the pulses were divided into probe and pump pulses (see Figure S1, supplemental information). Furthermore, a microscope objective lens (10×; NA = 0.25; Olympus, Japan) was used to focus the pump pulses to a spot that was located 10 μm below the side surface of a fused silica sample (polished on three sides, 10 mm × 10 mm × 0.5 mm). The 800-nm probe pulses were first passed through a one-dimensional linear stage (KA1000, Zolix, Inc, China) to adjust the time difference between the pump and probe pulses with a linear displacement accuracy of 1 μm. Subsequently, the probe pulses were frequency doubled to 400 nm by the BBO crystal. The 800- and 400-nm probe pulses were then emitted simultaneously. Next, the two probe pulses were passed through the birefringent quartz crystal to generate ordinary and extraordinary subpulses, namely 800-o, 800-e, 400-o, and 400-e subpulses. The four subpulses were irradiated in the area where the pump laser interacted with the sample and passed through an imaging objective (40×, NA = 0.4, Olympus, Japan). The two 800-nm subpulses and the two 400-nm subpulses were then spatially separated into two groups by using a dichroic mirror (cutoff wavelength = 560 nm). Subsequently, the pulses in each of the groups were further divided into individual subpulses with

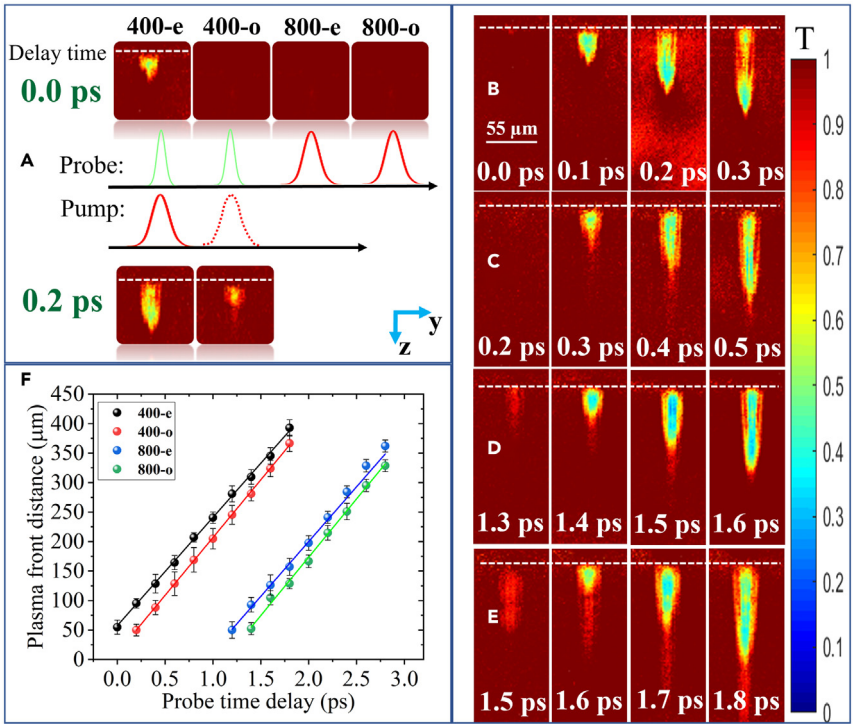

Figure 3. Measurement of subpulse intervals by using the multiframe imaging system

(A) Definition of time zero between the pump and probe pulses.

(B–E) Propagation of laser-induced plasma in fused silica was observed for the 400-e, 400-o, 800-e, and 800-o subpulses. The white dotted line represents the interface between air and the material. The colorbar T is the transmittance of the material to the probe pulses.

(F) Time evolution of the plasma front distance in fused silica.

different polarizations by using a polarization splitter. Finally, the probe subpulses were detected using four identical charge-coupled device (CCD) cameras (Imaging Source, DMK 23U445, Germany) to observe the interactions between the femtosecond laser pulse and the sample at different times. To ensure that different CCDs obtain images of the same size, we maintained a consistent distance between each CCD and the imaging objective, adjusted the size of the image through the imaging tube in front of the CCD, and ensured consistency in imaging for each CCD by measuring the number of pixel points.

RESULTS AND DISCUSSION

Measurement and analysis of the time shift between subpulses

We generated four probe subpulses with specific time delays by using the experimental setup displayed in Figure 2. We measured the time intervals between the subpulses according to the occurrence times of the same experimental phenomenon (i.e., plasma appearance) for each probe subpulse. In general, when a femtosecond pulse is focused on fused silica, the plasma is excited and gradually propagates inward.[27,28] Accordingly, observing the time evolution of plasma transmissivity is an effective method of measuring the time interval between subpulses. As illustrated in Figure 3A, the diameter of the pump was 8 mm. By adjusting the one-dimensional linear stage, we controlled the time delay between the probe subpulses and the pump pulse. According to the temporal sequence of the four subpulses, we identified the 0.0 ps when the fourth pulse (400-e) coincided with the pump pulse. At this time, the plasma in the fused silica was excited; however, the first three subpulses were not observed anything at this time because they were advanced in time than the 400-e. This is similar to when we choose the last person in the team (400-e) as the benchmark, who can see the plasma excited by the pump (the 800-nm pump pulse whose time not change), while the three in front are walking ahead and cannot see any information. When the team steps back a certain distance, the third place (400-o) can see the phenomenon. Therefore, when the one-dimensional linear stage was moved backward by 30 μm (0.2 ps), the third pulse (400-o) was captured in the same manner as the 400-e pulse. Therefore, we concluded that the time interval between the third and fourth pulses was 0.2 ps. Furthermore, we determined that the velocities of the plasma front for the first, second, third, and fourth pulses were 1.90×10^8, 1.93×10^8, 1.92×10^8, and 1.92×10^8 m/s, respectively (Figure 3F). Although the transmissivity of the excited plasma differed for different wavelengths, the calculated plasma propagation velocities were similar for all pulses and approximated the propagation velocity of light in the fused quartz (2.06×10^8 m/s). This result demonstrates the feasibility of the experimental setup.

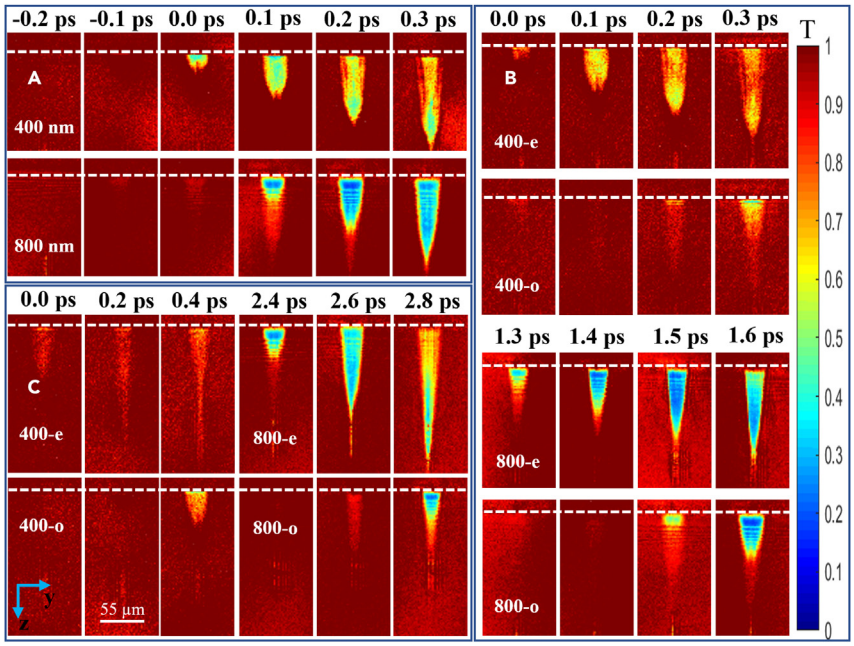

Figure 4. Pulse interval measurements were obtained by observing the time evolution of laser-induced plasma in material

(A) Time synchronization of 400- and 800-nm probes emitted from BBO.

(B) Time interval observed after subpulses passed through a 6.4-mm-thick quartz crystal.

(C) Time interval observed after subpulses passed through a 12.8-mm-thick quartz crystal.

The 0.2-ps time interval between the 400-o and 400-e subpulses (Figures 3B and 3C) was consistent for all polarizations at 400 nm. However, an assessment of the interval between the second subpulse (800-e) and the third subpulse (400-o) revealed that the plasma did not appear until 1.4 ps (see Figure S2, supplemental information, for additional details). Therefore, the delay between the 400-o and 800-e subpulses was 1.1 ps, which was inconsistent with that observed between the 400-o and 400-e subpulses, indicating that the group velocity difference between the two pulses changed considerably.

To explore factors contributing to the observed abnormal time delay, we first verified the synchronization of the 400- and 800-nm pulses without using the quartz crystal (i.e., the probe pulses passed through only the BBO crystal). As illustrated in Figure 4A, the laser-induced plasma in the fused silica affected the transmittance of the probe pulse (see Figure S3, supplemental information, for additional details). Under excitation with the 400-nm pulse, the plasma appeared at 0.0 ps and propagated inward. Because the pulse broadened after passing through multiple optical elements (i.e., it broadened to 115 fs; see Figure S4, supplemental information),[29] we moved the one-dimensional linear stage at steps of 15 μm (equivalent to a 100-fs time delay). Under excitation with the 800-nm pulse, although the plasma was not observed until 0.1 ps, it had already propagated inward for some distance. At 0.0 ps, weakly ionized plasma was also observed. This was attributed to the low plasma density in that early stage; the plasma detection sensitivity was higher for longer-wavelength light. This thus explains the time delay in the appearance of transmissivity between 400-nm excitation and 800-nm excitation. In summary, the 400- and 800-nm pulses emitted from the BBO crystal were synchronized, with the synchronization error being $\leq$0.1 ps.

According to the theory of light propagation in quartz crystals, the time interval between pulses increases linearly with the crystal thickness. Accordingly, we analyzed the differences in the time intervals between the four subpulses at different crystal thicknesses. At a crystal thickness of 6.4 mm (Figure 4B), assessing changes in the transmittance of the plasma revealed that the time interval between the 400-o and 400-e subpulses and that between the 800-o and 800-e subpulses were both approximately 0.2 ps. However, the time interval between the 400-e and 800-o subpulses was 1.1 ps. The darker colors in the figures are attributable to the low transmittance of the excited plasma under the 800-nm pulse. At a thickness of 12.8 mm (Figure 4C), the time interval between the 400-e and 800-o subpulses increased to 2.2 ps. The time intervals increased exponentially with the crystal thickness and followed a simple linear relationship.

When we changed the laser intensity, we observed that the time delay did not change. As displayed in Figure 5A, when the energy of the 400- and 800-nm pulses were 6.9 mJ/cm^2 and 960 mJ/cm^2, respectively, the plasma appeared after 0.2 ps under excitation with the 400-e subpulse and exhibited an obvious change in transmittance. Moreover, under the 400-o subpulse, the plasma appeared at 0.4 ps. However, under 800-e and 800-o subpulses, the plasma appeared at 1.5 ps and 1.7 ps, respectively. The time interval between pulses of the same wavelength was still 0.2 ps; however, that between the 800-e and 400-o subpulses was 1.1 ps. When the energy of the 400- and 800-nm pulses was increased to 14.8 mJ/cm^2 and 1420 mJ/cm^2, respectively (Figure 5C), the time intervals between the four subpulses remained unchanged. In particular, when the energy was doubled, the time intervals still remained unchanged (Figure 5E). These phenomena were obviously different from well-known nonlinear effects, which are closely related to the laser energy.

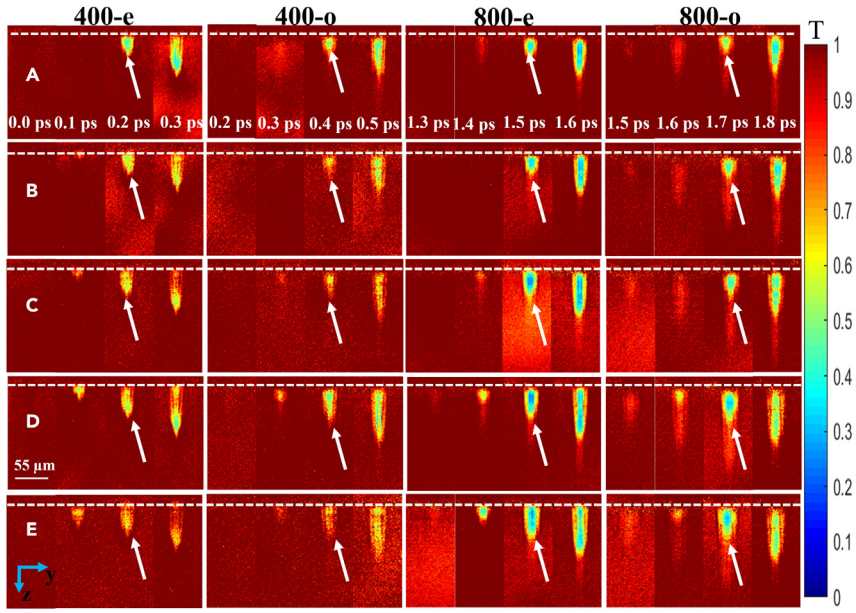

Figure 5. Time interval measurements for various probe pulse energy

(A) 6.9 mJ/cm^2 for 400-nm pulse, 960 mJ/cm^2 for 800-nm pulse.
(B) 10.2 mJ/cm^2 for 400-nm pulse, 1140 mJ/cm^2 for 800-nm pulse.
(C) 14.8 mJ/cm^2 for 400-nm pulse, 1420 mJ/cm^2 for 800-nm pulse.
(D) 17.0 mJ/cm^2 for 400-nm pulse, 1510 mJ/cm^2 for 800-nm pulse.
(E) 30.3 mJ/cm^2 for 400-nm pulse, 1990 mJ/cm^2 for 800-nm pulse.

Quartz is an anisotropic material; hence, the 800-nm pulse clearly caused a change in its properties. This change caused the strong dispersion of the 400-nm pulse traveling through the crystal, in addition to inducing a decrease in group velocity. As displayed in Figure 1D, when the 800-nm pulse passed through the quartz crystal, two 800-nm subpulses (i.e., 800-o and 800-e) were generated. We measured the time delay between these subpulses by using an autocorrelator (GECO, Light Conversion, Lithuania), as presented in Figures 6A and 6A. The time intervals between the 800-o and 800-e subpulses when they passed through the 6.4- and 12.8-mm-thick quartz crystals were approximately 200 and 400 fs, respectively, consistent with our calculations.

The quartz crystal is a wide bandgap material. In our experiment, the absorption of pump pulse should be caused by the nonlinear process of multi-photon absorption. The four probe pulses were used to observe the absorption process of the pump pulse. The probe pulse energy of 800 nm or 400 nm was much lower than the ionization threshold of quartz, making it impossible to excite plasma. Hence, the probe pulses should only have a small amount of energy absorbed by the crystal and most of the energy is transmitted through the crystal.[30] According to the Classical Thomson scattering,[31] electrons have scattering effects on low intensity light, and this is a linear process. The kinetic energy and photon frequency of free charged particles do not change due to scattering. Therefore, the time interval between 800-e and 400-o should be the theoretical calculated value. However, the time interval between them increased by 5 times than the theoretical calculated value according to our observation experiment, which indicated that this was not a simple linear relationship. And if this process was a nonlinear process, it should be closely related to pulse energy, and our experiments have shown that this time delay was independent of the pulse energy. Therefore, it was not a traditional nonlinear effect related to light intensity.[32] According to the experimental results, the 800-nm probe pulse ahead has an impact on the subsequent 400-nm pulses, causing a decrease in its speed. When a 400-nm pulse passes through, it appears to be coupled with the residual electromagnetic field of an 800-nm pulse. The delayed interaction between electric fields affects the propagation of 400-nm pulse, resulting in an increase in the time interval between 400-e and 800-o subpulses.

In Figure 5, the time delay is independent of laser intensity, thus representing weak light propagation. Light is an electromagnetic wave whose amplitude is the electric field strength.[33,34] In our experiments, the energy density of the pulses was considerably below the ionization threshold; hence, the intensity was unrelated to the laser propagation velocity. This phenomenon is similar to the phenomenon in which sunlight traveling at different intensities in the same medium maintains a constant velocity. Increasing the intensity of the 800-nm pulse increased the strength of the electric field caused by the excited electrons. This electric field in turn affected the intensity of the 400-nm pulse, but the time interval between the 400- and 800-nm pulses did not change. Two pulses of the same wavelength follow the birefringence effect. The oscillation frequency of the electric field excited by the 800-nm pulse affected electrons of a different frequency but did not affect those of the same frequency.[35] However, the interaction mechanism between these different frequencies should be further studied and explained.

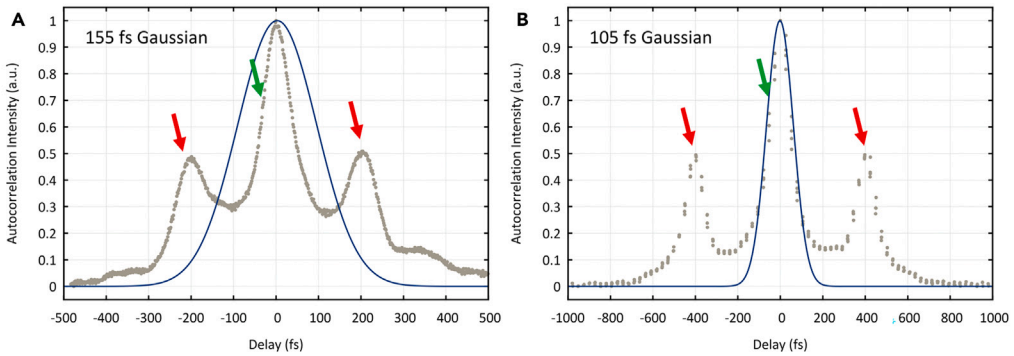

Figure 6. Measurement of pulse time intervals of 800-nm probe passing through quartz crystals of different thicknesses using an autocorrelator

(A) 6.4 mm crystal.

(B) 12.8 mm crystal. The green arrows represent the intensity of the superimposed 800nm o-ray, while the red arrows represent the 800nm e-ray.

Ultrafast multi-frame observation of femtosecond laser–induced shock waves

On the basis of the measured time intervals between the probe subpulses, we continually observed the time evolution process of femtosecond laser–induced shock waves. As shown in Figure 7, the laser fluence was 2.56 × 10^3 J/cm^2, and a single laser pulse was focused on the side surface of a fused quartz (polished on three sides: 10 mm × 10 mm × 0.5 mm) by using a 10× microscope objective lens. After being ablated, the sample was moved to a new position for the next pulse ablation, and meanwhile moved to a one-dimensional linear stage to obtain shock wave expansion morphology under different probe delays. We defined the time of initial appearance of plasma filaments generated by the breakdown of air as 0.0 ps (Figure 7B). Before the appearance of these filaments, a hemispherical plasma shock wave appeared.[36] When the laser pulse reached the surface of the material, the front of the pulse was reflected by the material surface. The air ionization threshold near the surface was reduced by two to three orders of magnitude.[37] The air molecules near the surface were ionized first, followed by those farther away. Moreover, when a femtosecond laser arrived at the sample surface, the laser energy was absorbed by the material within tens of femtoseconds. Subsequently, several free electrons were excited, and a small amount of plasma erupted from the material.[38] These two plasma materials formed shock waves. As the probe time delay increased, the plasma filaments interacted with the shock waves, forming two plasma waves propagating in opposite directions. Finally, owing to the continuous expansion of the material plasma shock waves, the two plasma waves were eventually squeezed and evolved into one plasma shock wave.

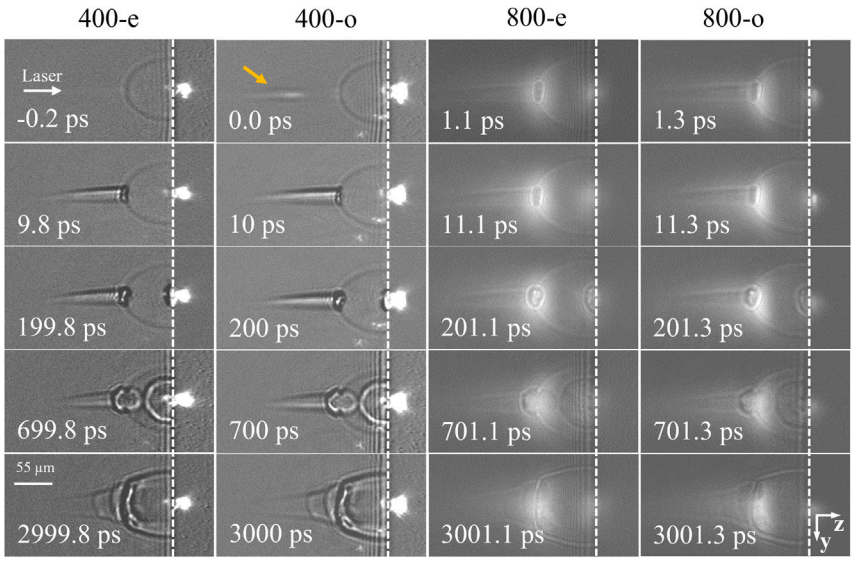

Figure 7. Single-shot multiframe observation of the femtosecond laser–induced shock wave

The same row represented the images captured by four CCDs under the same pump pulse excitation, while different rows represented the images obtained by pump pulse excitation at different probe delays. The yellow arrow represents the air plasma filament, and the white dotted line is the boundary between the air and the sample.

Conclusion

We have studied the evolution process of plasma filaments in a quartz crystal to measure the time shift of two-color probe pulses in the crystal. We observed that the 800-nm pulse changed the transient characteristics of the crystal. The internal dispersion characteristics of the 400-nm pulse had been enhanced. Therefore, the time delay between the 800-nm and 400-nm pulses was significantly increased compared to the calculated value based on dispersion theory. In addition, we observed that the abnormal time delay between these pulses was independent of pulse intensity, proving that it was not a traditional nonlinear effect related to light intensity ($\Delta n = 0$). One possibility is that the 800-nm pulse has some kind of residual electromagnetic field and affected the subsequent 400-nm pulse's propagation process. The delayed interaction between electric fields affects the transmission of the 400-nm pulse, increasing the time interval between 800-nm and 400-nm pulses. However, further research is needed on the true physical reasons and why this phenomenon is independent of pulse intensity. We performed single-shot multi-frame imaging experiments using pulse sequences with abnormal pulse delay effects, continuously observed the temporal evolution of laser-induced plasma shock waves, and determined the coupling process of multiple shock waves.

Limitations of the study

Here, we provided an experimental demonstration of the abnormal time delay of femtosecond laser pulses in a quartz crystal. Further experimental verification is needed to determine whether similar phenomena exist in other crystals. And the physical mechanism behind this abnormal time delay effect still needs further investigation.

STAR★METHODS

Detailed methods are provided in the online version of this paper and include the following:

- KEY RESOURCES TABLE
- RESOURCES AVAILABILITY
  - Lead contact
  - Materials availability
  - Data and code availability
- EXPERIMENTAL MODEL AND STUDY PARTICIPANT DETAILS
- METHOD DETAILS
- QUANTIFICATION AND STATISTICAL ANALYSIS

SUPPLEMENTAL INFORMATION

Supplemental information can be found online at https://doi.org/10.1016/j.isci.2024.110316.

ACKNOWLEDGMENTS

The authors acknowledge the National Key R&D Program of China (2023YFB4603203, 2022YFB4601300, 2022YFB4602900), National Natural Science Foundation of China (NSFC) (No. 51975054, 52375401), the Joint Funds of the National Natural Science Foundation of China (No. U2037205), the Chongqing Natural Science Foundation of China (grant cstc2021jcyj-cxttX0003, CSTB2022NSCQ-MSX1322).

AUTHOR CONTRIBUTIONS

B.S. G.: conceptualization; formal analysis; investigation; methodology; visualization; writing – review & editing; and project administration. T.Y. Z.: data curation; methodology; and writing – review and editing. L. J.: conceptualization; investigation; project administration; resources; supervision; and writing – review and editing.

DECLARATION OF INTERESTS

The authors declare no competing interests.

Received: January 24, 2024
Revised: May 31, 2024
Accepted: June 18, 2024
Published: June 19, 2024

REFERENCES

1. Carolan, J., Harrold, C., Sparrow, C., Martín-López, E., Russell, N.J., Silverstone, J.W., Shadbolt, P.J., Matsuda, N., Oguma, M., Itoh, M., et al. (2015). QUANTUM OPTICS. Universal linear optics. Science *349*, 711–716. https://doi.org/10.1126/science.aab3642.
2. Knill, E., Laflamme, R., and Milburn, G.J. (2001). A scheme for efficient quantum computation with linear optics. Nature *409*, 46–52. https://doi.org/10.1038/35051009.
3. Boonserm, P., Cattoen, C., Faber, T., Visser, M., and Weinfurtner, S. (2005). Effective refractive index tensor for weak-field gravity.

Class. Quantum Gravity *22*, 1905–1915. https://doi.org/10.1088/0264-9381/22/11/001.
4. Wang, P. (2021). Group velocity of light in uniaxial crystals. Appl. Opt. *60*, 1987–1994. https://doi.org/10.1364/AO.416686.
5. Peters, P.F.A.H.C., and Weinreich, G. (1961). Generation of optical harmonics. Phys. Rev. Lett. *7*, 118–119. https://doi.org/10.1103/physrevlett.7.118.
6. Adair, R., Chase, L., and Payne, S.A. (1989). Nonlinear refractive index of optical crystals. Phys. Rev. B *39*, 3337–3350. https://doi.org/10.1103/PhysRevB.39.3337.
7. Fournier, J., and Snitzer, E. (1974). The nonlinear refractive index of glass. IEEE J. Quantum Electron. *10*, 473–475. https://doi.org/10.1109/jqe.1974.1068176.
8. Wang, X., He, P., Yan, L., Si, J., Chen, F., and Hou, X. (2013). Pump power dependence of the spatial gating properties of femtosecond optical Kerr effect measurements. Appl. Phys. B *112*, 279–283. https://doi.org/10.1007/s00340-013-5431-4.
9. Alexandridi, C., Délen, X., Druon, F., Georges, P., Martin, L., Mathieu, F., and Papadopoulos, D. (2021). Generation of optically synchronized pump–signal beams for ultrafast OPCPA via the optical Kerr effect. Opt. Lett. *46*, 2035–2038. https://doi.org/10.1364/ol.425237.
10. Vampa, G., Hammond, T.J., Nesrallah, M., Naumov, A.Y., Corkum, P.B., and Brabec, T. (2018). Light amplification by seeded Kerr instability. Science *359*, 673–675. https://doi.org/10.1126/science.aaq0053.
11. Guo, X., Ding, Y., Duan, Y., and Ni, X. (2019). Nonreciprocal metasurface with space–time phase modulation. Light Sci. Appl. *8*, 123. https://doi.org/10.1038/s41377-019-0225-z.
12. Ho, P.P., and Alfano, R.R. (1979). Optical Kerr effect in liquids. Phys. Rev. *20*, 2170–2187. https://doi.org/10.1103/PhysRevA.20.2170.
13. Tan, W., Ma, J., Si, J., Huang, Z., and Hou, X. (2022). Femtosecond optical Kerr gate with double gate pulses: Simulation and experiment. Opt. Laser Technol. *145*, 107531. https://doi.org/10.1016/j.optlastec.2021.107531.
14. Michel, A.-K.U., Zalden, P., Chigrin, D.N., Wuttig, M., Lindenberg, A.M., and Taubner, T. (2014). Reversible optical switching of infrared antenna resonances with ultrathin phase-change layers using femtosecond laser pulses. ACS Photonics *1*, 833–839. https://doi.org/10.1021/ph500121d.
15. Harris, S.E., Field, J., and Imamoğlu, A. (1990). Nonlinear optical processes using electromagnetically induced transparency. Phys. Rev. Lett. *64*, 1107–1110. https://doi.org/10.1103/physrevlett.64.1107.
16. Zhu, L., and Dong, L. (2022). Electromagnetically induced transparency metamaterials: theories, designs and applications. J. Phys. D. Appl. Phys. *55*, 263003. https://doi.org/10.1088/1361-6463/ac60cc.
17. Bigelow, M.S., Lepeshkin, N.N., and Boyd, R.W. (2003). Superluminal and slow light propagation in a room-temperature solid. Science *301*, 200–202. https://doi.org/10.1126/science.1084429.
18. Bigelow, M.S., Lepeshkin, N.N., and Boyd, R.W. (2003). Observation of ultraslow light propagation in a ruby crystal at room temperature. Phys. Rev. Lett. *90*, 113903. https://doi.org/10.1103/PhysRevLett.90.113903.
19. Hahn, J., and Ham, B.S. (2008). Observations of self-induced ultraslow light in a persistent spectral hole burning medium. Opt. Express *16*, 16723–16728. https://doi.org/10.1364/oe.16.016723.
20. Turukhin, A.V., Sudarshanam, V.S., Shahriar, M.S., Musser, J.A., Ham, B.S., and Hemmer, P.R. (2002). Observation of ultraslow and stored light pulses in a solid. Phys. Rev. Lett. *88*, 023602. https://doi.org/10.1103/PhysRevLett.88.023602.
21. Zhang, J.-y., Huang, J.Y., Wang, H., Wong, K., and Wong, G. (1998). Second-harmonic generation from regeneratively amplified femtosecond laser pulses in BBO and LBO crystals. JOSA B *15*, 200–209. https://doi.org/10.1364/josab.15.000200.
22. Jundt, D.H. (1997). Temperature-dependent Sellmeier equation for the index of refraction, n_e, in congruent lithium niobate. Opt. Lett. *22*, 1553–1555. https://doi.org/10.1364/OL.22.001553.
23. Liu, H., Chen, G., Zhao, W., Wang, Y., Wang, T., and Zhao, S. (2001). Phase matching analysis of noncollinear optical parametric process in nonlinear anisotropic crystals. Opt. Commun. *197*, 507–514. https://doi.org/10.1016/s0030-4018(01)01475-4.
24. Akbari, R., and Major, A. (2013). Optical, spectral and phase-matching properties of BIBO, BBO and LBO crystals for optical parametric oscillation in the visible and near-infrared wavelength ranges. Laser Phys. *23*, 035401. https://doi.org/10.1088/1054-660x/23/3/035401.
25. Ghosh, G. (1999). Dispersion-equation coefficients for the refractive index and birefringence of calcite and quartz crystals. Opt. Commun. *163*, 95–102. https://doi.org/10.1016/s0030-4018(99)00091-7.
26. Hayata, K., and Koshiba, M. (1993). Group-velocity-matched second-harmonic generation: An efficient scheme for femtosecond ultraviolet pulse generation in periodically domain-inverted β-BaB_2O_4. Appl. Phys. Lett. *62*, 2188–2190. https://doi.org/10.1063/1.109464.
27. Sun, Q., Jiang, H., Liu, Y., Wu, Z., Yang, H., and Gong, Q. (2005). Measurement of the collision time of dense electronic plasma induced by a femtosecond laser in fused silica. Opt. Lett. *30*, 320–322. https://doi.org/10.1364/ol.30.000320.
28. Pan, C., Jiang, L., Sun, J., Wang, Q., Wang, F., and Lu, Y. (2019). The temporal-spatial evolution of electron dynamics induced by femtosecond double pulses. Jpn. J. Appl. Phys. *58*, 030901. https://doi.org/10.7567/1347-4065/ab00a8.
29. Vardanyan, A., Mailyan, A., and Oganesyan, D. (1997). Focusing of femtosecond light pulses with a lens. Opt. Spectrosc. *82*, 416–419. https://www.researchgate.net/publication/259357903.
30. Jiang, L., Wang, A.-D., Li, B., Cui, T.-H., and Lu, Y.-F. (2018). Electrons dynamics control by shaping femtosecond laser pulses in micro/nanofabrication: modeling, method, measurement and application. Light Sci. Appl. *7*, 17134. https://doi.org/10.1038/lsa.2017.134.
31. Chen, S.-y., Maksimchuk, A., and Umstadter, D. (1998). Experimental observation of relativistic nonlinear Thomson scattering. Nature *396*, 653–655. https://doi.org/10.1038/25303.
32. Schiffrin, A., Paasch-Colberg, T., Karpowicz, N., Apalkov, V., Gerster, D., Mühlbrandt, S., Korbman, M., Reichert, J., Schultze, M., Holzner, S., et al. (2013). Optical-field-induced current in dielectrics. Nature *493*, 70–74. https://doi.org/10.1038/nature11567.
33. Kuratsuji, H., and Kakigi, S. (1998). Maxwell-Schrödinger equation for polarized light and evolution of the Stokes parameters. Phys. Rev. Lett. *80*, 1888–1891. https://doi.org/10.1103/PHYSREVLETT.80.1888.
34. Lee, D.G., Kim, J.-H., Hong, K.-H., and Nam, C.H. (2001). Coherent control of high-order harmonics with chirped femtosecond laser pulses. Phys. Rev. Lett. *87*, 243902. https://doi.org/10.1117/12.425656.
35. Cui, C., Jin, R., Jiang, D., Zhang, J., and Zhu, J. (2021). Visualization of an Accelerated Electrochemical Reaction under an Enhanced Electric Field. Research *2021*, 1742919. https://doi.org/10.1364/OE.23.001370.
36. Zhang, H., Zhang, F., Du, X., Dong, G., and Qiu, J. (2015). Influence of laser-induced air breakdown on femtosecond laser ablation of aluminum. Opt. Express *23*, 1370–1376.
37. Hu, W., Shin, Y.C., and King, G. (2011). Early-stage plasma dynamics with air ionization during ultrashort laser ablation of metal. Phys. Plasmas *18*, 093302. https://doi.org/10.1063/1.3633067.
38. Axente, E., Noël, S., Hermann, J., Sentis, M., and Mihailescu, I.N. (2009). Subpicosecond laser ablation of copper and fused silica: Initiation threshold and plasma expansion. Appl. Surf. Sci. *255*, 9734–9737. https://doi.org/10.1016/j.apsusc.2009.04.060.

STAR★METHODS

KEY RESOURCES TABLE

REAGENT or RESOURCE	SOURCE	IDENTIFIER
Chemicals, peptides, and recombinant proteins		
Quartz birefringent crystal	Fujian Ultra Photonics Co., Ltd.	https://www.u-photonics.com/
Fused silica	HeFei Crystal Technical Material Co.,Ltd.	http://www.ctmwafer.com/

RESOURCES AVAILABILITY

Lead contact

Further information and requests for resources and reagents should be directed to and will be fulfilled by the Lead Contact, Baoshan Guo (gbs@bit.edu.cn).

Materials availability

This study did not generate new unique reagents.

Data and code availability

- All data reported in this paper will be shared by the lead contact upon request.
- This paper does not report original code.
- Any additional information required to reanalyze the data reported in this paper is available from the lead contact upon request.

EXPERIMENTAL MODEL AND STUDY PARTICIPANT DETAILS

Our study does not use experimental models typical in the life sciences.

METHOD DETAILS

As illustrated in Figure 2, it shows the configuration of the multifrequency pulse framing imaging system. We introduce in detail how to adjust the optical components and to ensure their mutual cooperation, which can be used to control the time interval between the four subpulses more precisely. First, the function of the polarization beam splitter is to separate two linearly polarized lasers that are perpendicular to each other. Therefore, the S-polarized laser (the polarization vector is perpendicular to the plane determined by the incident laser and the reflected laser) is reflected at an angle of 45°, and the P-polarized laser (the polarization vector is in the plane) is simultaneously transmitted. Because the lasers in the entire system propagate in the same horizontal plane, the mirror surface is perpendicular to the laser propagation plane; that is, the S-polarized laser is vertically linearly polarized, and the P-polarized laser is horizontally linearly polarized. Therefore, the perpendicular subpulses with wavelengths of 400 nm and 800 nm from the uniaxial quartz crystal must be horizontally polarized and vertically polarized, respectively. However, according to the birefringence phenomenon of the uniaxial quartz crystal, which occurs when a linearly polarized laser is incident perpendicular to the mirror surface and forms an angle of 45° with the optical axis (in the mirror surface), the vibration direction of the emitted extraordinary laser (e-ray) coincides with the optical axis, and the vibration direction of the ordinary laser (o-ray) is perpendicular to the optical axis. Therefore, to ensure that the final polarization directions of the pulses match those of the polarization beam splitter, the optical axis of the quartz crystal is adjusted to be vertical; at the same time, the angle between the polarization state of 400 nm e-ray and the horizontal line is required to rotate 45° counterclockwise. Therefore, the angle between the optical axis of the BBO crystal (in the mirror) and the horizontal line is also rotated 45° counterclockwise. According to calculations in the previous section, when the polarization vector angle between the BBO crystal and the linearly polarized laser is 29.2°, the phase matches; therefore, the angle between the initial fundamental-frequency laser (800 nm linearly polarized) and the vertical line is 15.8° clockwise. The specific beam splitting propagation process is displayed in Figure 1E. According to the order of time, the first and last beams are 800-nm o-ray, 800-nm e-ray, 400-nm o-ray, and 400-nm e-ray.

QUANTIFICATION AND STATISTICAL ANALYSIS

The Origin2018 was used for statistical analysis. The transmittance of the material to the probe pulses was calculated using Matlab R2018b.